Performance of the ionospheric kappa-correction of radio occultation profiles under diverse ionization and solar activity conditions

Julia Danzer[1], Stephanie Juliane Haas[2], Marc Schwaerz[3], and Gottfried Kirchengast[3]

[1]Wegener Center for Climate and Global Change, University of Graz
[2]Wegener Center for Climate and Global Change
[3]University of Graz

November 22, 2022

Abstract

The kappa-correction is an easy-to-use method to correct for residual ionospheric errors in radio occultation (RO) data. It is a simple empirical model term that only depends on readily available data. While its basic utility was well proven in previous studies, including a recent predecessor study on RO climatologies under solar cycle variations, its performance for individual RO profile correction under diverse and extreme ionization conditions is unclear so far. Here we tackle this gap and focus on investigating (extremely) low and high solar activity and ionization conditions of individual RO events, including inspection of ionospheric symmetry between inbound and outbound raypaths. Using a global multi-year ensemble of MetOp-A and GRACE-A RO events over 2008 to 2015 as basis, we applied a sampling approach leading to six characteristic condition cases. These cases also relate to day and night time variations and geographic variations from the equatorial to the high latitude region. We inspected the kappa-correction and its performance relative to the standard bending angle correction for RO-retrieved stratospheric profiles and found mean deviations in temperature of near -0.3K in the upper stratosphere 40-45km for high ionization conditions, with extreme deviations exceeding -2K for strong inbound/outbound asymmetry. The kappa-correction term itself reaches a mean value near 0.05µrad under these high conditions. Low solar activity and ionization conditions lead to a mean correction smaller than 0.005µrad and mean temperature deviations smaller than 0.02K. An intercomparison to other quality datasets, predominantly showed a decrease in mean temperature difference when applying the kappa-correction.

Performance of the ionospheric kappa-correction of radio occultation profiles under diverse ionization and solar activity conditions

J. Danzer[1], S. J. Haas[1], M. Schwaerz[1], G. Kirchengast[1,2]

[1]Wegener Center for Climate and Global Change (WEGC), University of Graz, Graz, Austria
[2]Institute of Physics, NAWI Graz, University of Graz, Graz, Austria

Key Points:

- The kappa-correction of radio occultation profiles is explored for low and high ionization, solar activity, and asymmetry
- The mean correction is most relevant under high ionization and symmetry, reaching near $0.05\,\mu$rad around $50\,$km
- Intercomparison with other datasets shows it predominantly decreases retrieved stratospheric temperature errors

Corresponding author: Julia Danzer, `julia.danzer@uni-graz.at`

Abstract

The kappa-correction is an easy-to-use method to correct for residual ionospheric errors in radio occultation (RO) data. It is a simple empirical model term that only depends on readily available data. While its basic utility was well proven in previous studies, including a recent predecessor study on RO climatologies under solar cycle variations, its performance for individual RO profile correction under diverse and extreme ionization conditions is unclear so far. Here we tackle this gap and focus on investigating (extremely) low and high solar activity and ionization conditions of individual RO events, including inspection of ionospheric symmetry between inbound and outbound raypaths. Using a global multi-year ensemble of MetOp-A and GRACE-A RO events over 2008 to 2015 as basis, we applied a sampling approach leading to six characteristic condition cases. These cases also relate to day and night time variations and geographic variations from the equatorial to the high latitude region. We inspected the kappa-correction and its performance relative to the standard bending angle correction for RO-retrieved stratospheric profiles and found mean deviations in temperature of near -0.3 K in the upper stratosphere (40-45 km) for high ionization conditions, with extreme deviations exceeding -2 K for strong inbound/outbound asymmetry. The kappa-correction term itself reaches a mean value near 0.05 μrad under these high conditions. Low solar activity and ionization conditions lead to a mean correction smaller than 0.005 μrad and mean temperature deviations smaller than 0.02 K. An intercomparison to other quality datasets, predominantly showed a decrease in mean temperature difference when applying the kappa-correction.

1 Introduction

Over the past years the global navigation satellite system (GNSS) radio occultation (RO) technique (Kursinski et al., 1997; Hajj et al., 2002) has become of increasing importance for climate and meteorological applications (e.g., A. Steiner et al., 2001; Anthes, 2011; A. Steiner et al., 2011; Healy & Thépaut, 2006; Cardinali, 2009; Cucurull, 2010). It provides a continuous record of near-vertical geophysical data profiles, since the launch of the CHAllenging Minisatellite Payload (CHAMP) mission in the year 2001 (e.g., Wickert et al., 2001; Ao et al., 2003; Foelsche et al., 2003). RO data show highest accuracy in the upper troposphere and lower stratosphere between about 5 km to 35 km (e.g., Kursinski et al., 1997; Foelsche et al., 2011; Zeng et al., 2019).

Towards increasing altitudes, RO bending angles have a decreasing signal-to-noise ratio, due to an increasing impact of measurement noise and ionospheric refraction in the data. In the retrieval processing chain, the related errors propagate downward from RO bending angle (α) to refractivity (N), pressure (p), and temperature (T) (Rieder & Kirchengast, 2001; A. K. Steiner & Kirchengast, 2005; Gobiet et al., 2007; Ho et al., 2012; A. Steiner et al., 2013; Schwarz et al., 2017, 2018). In this specific work, data quality is increased in the middle and upper stratosphere by applying a second-order ionospheric correction on the bending angle profiles (Healy & Culverwell, 2015), the so-called kappa-correction. The focus lies on understanding the second-order impact on the dry atmospheric RO parameters (α, N, p, T), and investigating its variation under diverse and extreme solar activity and ionization conditions, since this is an important gap left by previous studies (introduced further below).

The primary measured quantity in the RO technique is the excess phase path profiles at the two Global Positioning Satellites L-band carrier frequencies, $f_1 = 1575.42$ MHz and $f_2 =$1227.60 MHz. From these excess phase profiles the bending angle profiles α_{L_1} and α_{L_2} can be derived, which are then combined using a dual-frequency linear combination of the RO bending angles, in order to correct for the influence of the ionosphere to first-order (Vorob'ev & Krasil'nikova, 1994; Ladreiter & Kirchengast, 1996). The remaining higher-order residual ionospheric errors (RIE) in the RO data are of increasing importance with increasing altitude (above about 35 km); furthermore they vary (mainly) with the diurnal and solar cycle, (e.g., Syndergaard, 2000; Mannucci et al., 2011; Danzer et al., 2013; Liu et al., 2013, 2015, 2018). Earlier approaches for higher-order ionospheric corrections exist, (e.g., Syndergaard, 2002; Kedar et al., 2003; Hoque & Jakowski, 2008; Vergados & Pagiatakis, 2010, 2011), however, they are usually in need of additional background information, such as the total electron content (TEC).

More recently a second-order ionospheric correction was introduced by Healy and Culverwell (2015), the so-called kappa-correction, which was at the same time also evaluated through simulation studies by Danzer et al. (2015). The kappa-correction in its simple functional-model form, introduced by Angling et al. (2018) as an advancement to Healy and Culverwell (2015), has the advantage of only needing the $F_{10.7}$ index as auxiliary background information. Otherwise, it just depends on the retrieved α_{L_1} and α_{L_2} bending angle profiles, which are available from the RO processing, and the location and time of the RO profile data, capturing location- and time-dependent solar variations.

In a recent predecessor study by Danzer et al. (2020), that used longer-term real RO data, the correction was tested for its influences on RO-derived climatologies as well as validated against reanalysis datasets. Analyzing 10° zonal-mean climatologies from the solar minimum year 2008 to the solar maximum year 2014, the study found that the kappa-correction generally warms the RO temperature climatology data. Furthermore, it showed a sensitivity of the kappa-correction of less than 0.2 K for low and more than 0.6 K for high solar activity conditions, in a middle stratosphere layer (30-35 km), with the largest correction over the tropics (20°S-20°N). The validation analysis showed that it is challenging to validate small improvements of RO data; datasets used were from the European Centre for Medium-Range Weather Forecasts (ECMWF) reanalyses ERA-Interim (Dee et al., 2011) and ERA5 (Hersbach et al., 2018, 2020). It was found difficult to discern small improvements in the RO data, since the validation datasets also feature small biases that are of similar magnitude as the ionospheric RIE correction term. The problem of validating improvements with other datasets will likely continue for other proposed changes to GNSS RO processing in the future.

Another recent study by Liu et al. (2020) provided a first assessment of a further advanced higher-order RIE correction, the so-called bi-local correction (Syndergarrd & Kirchengast, 2019), which on top of the kappa-correction's scope accounts also for the geomagnetic higher-order term, the finite RO receiver orbit altitude, and ionospheric inbound/outbound asymmetry. It requires significantly more auxiliary background information, such as the TEC for the inbound and outbound regions of each RO event. The initial intercomparison of the bi-local correction with the kappa-correction under different ionization conditions by Liu et al. (2020) showed that the latter is, in spite of its simplicity, generally very comparable and consistent with the more advanced correction, with limits reached for smaller-scale averages and under individual-event conditions that are not captured by its more simplified formulation. Hence, it is valuable to further explore the kappa-correction performance especially also for diverse and extreme solar and ionization conditions.

In this study we focus on a kappa-correction performance analysis based on ensembles of individual RO events, applying a targeted subset-sampling approach to a large global multi-year ensemble of RO data. The concept is to subsample all profiles that occur beyond particular thresholds of solar activity (measured in daily $F_{10.7}$ values), ionization level (measured in vertical total electron content vTEC), and degree of inbound/outbound asymmetry (measured by an asymmetry factor f_{IA} introduced in section 2). More specifically, we use all MetOp-A and GRACE-A RO events from the years 2008 to 2015 as basis, from which we subsample those which occurred during specific high and low $F_{10.7}$, vTEC, and f_{IA} conditions.

This approach has the advantage to extract robust subsets of RO profile data for ensemble inspection and statistical analysis under very distinct ambient conditions of interest. Furthermore it intrinsically samples the diurnal (local time) cycle and the equatorial to midlatitude to polar regions in a characteristic and insightful way (as seen in section 2 on methods and datasets).

Hence the approach enables to inspect the performance of the kappa-correction explicitly under low and high solar activity, ionization, and asymmetry conditions and implicitly under diurnal and solar cycle variations as well as geographical variations, capturing the most salient temporal and spatial variations of the ionosphere. Closer analysis of these specific variations of RIEs was recommended also in International Radio Occultation Working Group (IROWG) climate subgroup recommendations (`https://irowg.org/irowg7_minutes_summary/`, last access 28 October 2020). This study therefore contributes also to meet this recommendation.

The paper is structured as follows. After introducing the method and datasets in section 2 we investigate and discuss the kappa-correction's performance related to RO bending angle, refractivity, pressure, and temperature profiles (section 3.1, complemented also by detailed result summary tables in Appendix A. The kappa-correction is afterwards validated against other datasets from ERA5 and ERA-Interim reanalyses (section 3.2). Conclusions are drawn in section 4.

2 Method and Datasets

The impact of the ionosphere on the RO profiles is basically corrected in the Wegener Center (WEGC) RO processing that is employed here by applying the first-order ionospheric bending angle correction given by Vorob'ev and Krasil'nikova (1994), also referred to as 'standard correction' hereafter:

$$\alpha_c(z_a) = \alpha_{L_1}(z_a) + \frac{f_2^2}{f_1^2 - f_2^2}[\alpha_{L_1}(z_a) - \alpha_{L_2}(z_a)] \ . \tag{1}$$

In this equation α_c is the estimate of the neutral atmosphere bending angle, and α_{L_1} and α_{L_2} are the L_1 and L_2 bending angles related to the frequencies f_1 and f_2, given at impact altitude z_a. Healy and Culverwell (2015) proposed a modification to the standard ionospheric correction, with an additional (positive) term to compensate for the higher-order ionospheric error:

$$\alpha_c(z_a, t) = \alpha_{L_1}(z_a) + \frac{f_2^2}{f_1^2 - f_2^2}[\alpha_{L_1}(z_a) - \alpha_{L_2}(z_a)] + |\kappa(z_a, t)| \cdot [\alpha_{L_1}(z_a) - \alpha_{L_2}(z_a)]^2 \ . \tag{2}$$

The latter term is the kappa-correction term, depending only on a slowly varying kappa factor $\kappa(z_a, t)$, and the α_{L_1} and α_{L_2} bending angle profile difference squared, which approximately models the dominant residual ionospheric variation from profile to profile. The kappa factor $\kappa(z_a, t)$ ([rad^{-1}]) is expressed by Angling et al. (2018):

$$\kappa(z_a, t) = a + b \cdot \mathrm{F}_{10.7}(t) + c \cdot \chi(t) + e \cdot z_a \ . \tag{3}$$

Hence it depends on the $\mathrm{F}_{10.7}$ index, given in solar flux units [sfu], and on the solar zenith angle $\chi(t)$, given in [rad], which contains the information of local time, season, and location of a profile. Furthermore, the kappa factor exhibits a slow altitudinal variation represented by the dependence on impact altitude z_a. a, b, c, e are regression coefficients found by fitting the model to large datasets (Angling et al., 2018).

2.1 Sampling approach and characteristic condition cases

In order to analyze the impact of the natural ionospheric variations on the residual ionospheric error (RIE), we apply a sampling approach on the individual RO profiles. The goal is to assess diurnal cycle, solar cycle, and geographical variations, as well as ionospheric raypath inbound and outbound asymmetry effects, on the kappa-correction.

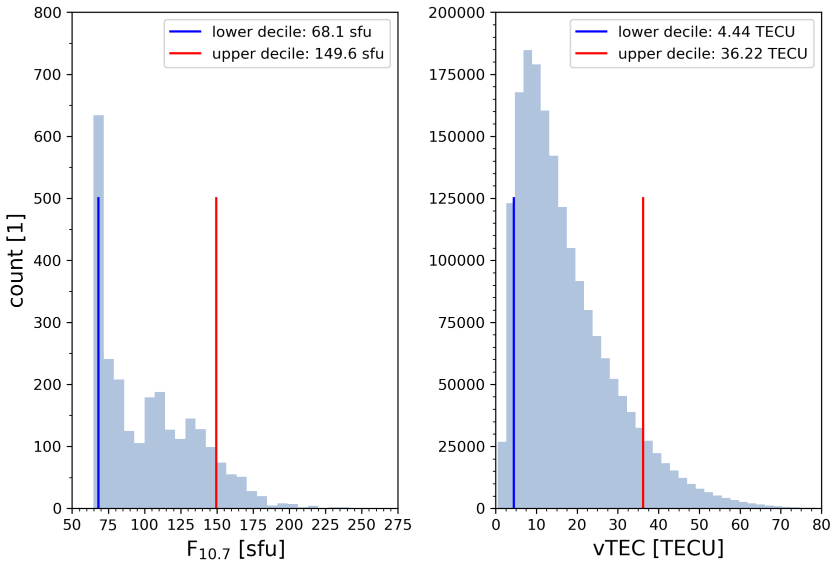

Figure 1. Histogram of the daily $F_{10.7}$ index values (left) and RO-event-collocated vTEC values (right), supporting the definition of the condition classes (Table 2), using the data from the solar minimum year 2008 up to the solar maximum year 2014. The blue and red lines mark the lower (blue) and upper (red) decile (i.e., 10 % and 90 % percentiles).

As a first diagnostic plot we inspect daily $F_{10.7}$ values (unit [sfu], $1\text{sfu} = 10^{-22}\text{Wm}^{-2}\text{Hz}^{-1}$) from the solar minimum year 2008 up to the solar maximum year 2014 (Figure 1, left panel). We intend to find the lower and upper 10 % (decile) of days within the minimum to the maximum of the solar cycle, in order to distinguish low solar activity from high solar activity. (In the later analysis plots when investigating RO data, we also include the year 2015 in the data range, in order to achieve a high profile statistics.) We round the results for the two deciles to $F_{10.7} = 70$ sfu, and classify all days up to this value as low solar activity days, while days with $F_{10.7} = 150$ sfu or higher are classified as high solar activity days. We apply the same diagnostics to the electron density, for classifying into low and high ionization conditions, by using the information of vTEC (unit [TECU], 1 TECU= 10^{16} electrons per m^2) (Figure 1, right panel). From these results we choose for the subset sampling event-collocated vTEC values of vTEC= 5 TECU and below for classifying RO events into low ionization conditions and vTEC values of vTEC= 35 TECU and higher for classifying into high ionization conditions, respectively.

Since the standard first-order ionospheric correction does not account for large-scale horizontal electron density gradients in the ionosphere along the GNSS signal's inbound and outbound raypaths, we also distinguish inbound/outbound-symmetric and -asymmetric conditions. Figure 2 illustrates the vTEC between inbound (from GNSS transmitter) and outbound (towards LEO receiver), respectively, defined as vTEC_{Tx} (inbound, x-axis) and vTEC_{Rx} (outbound, y-axis), respectively. For enabling classification into nearly-symmetric and strongly asymmetric cases we used the following formal definition of an ionospheric asymmetry factor, in line with Liu et al. (2020):

$$f_{IA}[\%] = 100 \cdot \frac{\text{vTEC}_{Tx} - \text{vTEC}_{mean}}{\text{vTEC}_{mean}} \,, \tag{4}$$

where $\text{vTEC}_{mean} = 0.5 \cdot (\text{vTEC}_{Tx} + \text{vTEC}_{Rx})$, and f_{IA} is the ionospheric asymmetry factor. A deviation of $|f_{IA}| \leq 10$ % from the average inbound-outbound vTEC is

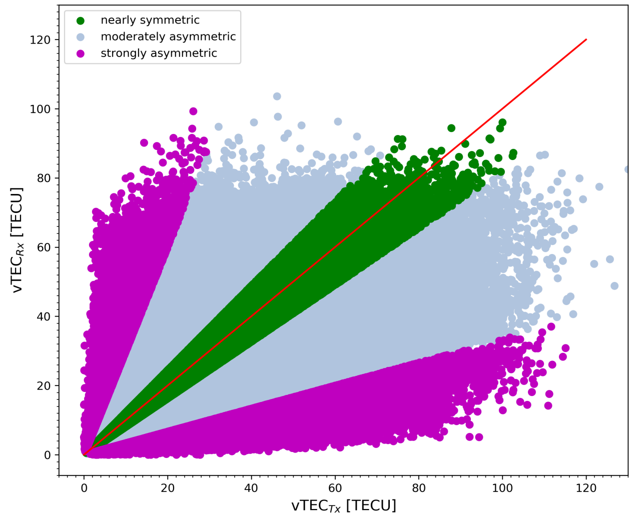

Figure 2. Scatter plot of the electron density showing inbound (vTEC$_{Tx}$) versus outbound (vTEC$_{Rx}$) conditions for the MetOp-A data over 2008-2014. The colors classify the ionospheric conditions, according to Eq. 2.2, into nearly symmetric (green), moderately asymmetric (blue), and strongly asymmetric (purple) RO event sub-ensembles.

used to classify RO events into nearly symmetric conditions, while a deviation of $|f_{IA}| \geq 50$ % comprises those under strongly asymmetric conditions.

Table 1. Definition of solar, ionization, and asymmetry conditions.

Parameter	Weak Condition	Strong Condition
$F_{10.7}$ [sfu]	$\leq$ 70 sfu, low solar activity	$\geq$ 150 sfu, high solar activity
vTEC [TECU]	$\leq$ 5 TECU, low ionization	$\geq$ 35 TECU, high ionization
$|f_{IA}|$ [%]	$\leq$ 10 %, nearly symmetric	$\geq$ 50 %, strongly asymmetric

To summarize, we sample RO profiles according to the three condition parameters, $F_{10.7}$ index, vTEC value, and f_{IA} factor, which is covered by the definition of conditions collected in Table 1. This leads to combinations of 8 different ensemble cases, summarized in Table 2. Since low $F_{10.7}$ conditions do essentially not mix with the occurrence of high vTEC values (Figure 3, bottom row), we practically end up with 6 characteristic condition cases, distinguished by their ionization and solar activity level, with the advantage of a rather large ensemble of RO profiles for each case.

Figure 3 also illustrates the geographical mapping of all six characteristic condition cases. The HiF$_{10.7}$-HiTEC-Sym/Asym cases (first row) occur primarily between about ±60°N/S, while the LoF$_{10.7}$-LoTEC-Sym/Asym cases (second row) do not occur over the equatorial region, but exist up to the northern and southern poles. The same is also true for the mixed cases of HiF$_{10.7}$-LoTEC-Sym/Asym (third row).

Finally Figure 3 also illustrates, as a further information, the local time of each RO event by way of a gradual color bar. This indicates that we clearly observe a diurnal cycle mapping for the six characteristic condition cases. The HiF$_{10.7}$-HiTEC-Sym/Asym cases strongly relate to daytime conditions, especially under ionospheric inbound/outbound

Table 2. Definition of characteristic condition cases. As shown in column 2, which gives the number of MetOp-A events complemented by the number of GRACE-A events in parentheses, the cases LoF$_{10.7}$-HiTEC-Sym/Asym exhibit a very small ensemble size (see also Figure 3). These cases are therefore dismissed in the following analysis. The total sample size of MetOp-A (GRACE-A) profiles is ∼1458100 (∼323100) profiles from 2008 to 2015, so small fractions ($< 0.1\,\% - 2\,\%$) of well-defined extreme conditions are isolated here.

Case Name	No. of Events	Description
HiF$_{10.7}$-HiTEC-Sym	6156 (624)	high solar activity, high ionization, nearly symmetric
HiF$_{10.7}$-HiTEC-Asym	8875 (1690)	high solar activity, high ionization, strongly asymmetric
LoF$_{10.7}$-LoTEC-Sym	6413 (639)	low solar activity, low ionization, nearly symmetric
LoF$_{10.7}$-LoTEC-Asym	23908 (3756)	low solar activity, low ionization, strongly asymmetric
HiF$_{10.7}$-LoTEC-Sym	515 (43)	high solar activity, low ionization, nearly symmetric
HiF$_{10.7}$-LoTEC-Asym	4005 (539)	high solar activity, low ionization, strongly asymmetric
LoF$_{10.7}$-HiTEC-Sym	3 (0)	low solar activity, high ionization, nearly symmetric
LoF$_{10.7}$-HiTEC-Asym	46 (58)	low solar activity, high ionization, strongly asymmetric

symmetry, and are rare at polar latitudes. On the other hand, the LoF$_{10.7}$-LoTEC-Sym/Asym cases show a majority of nighttime events with low vTEC values and are rare at equatorial latitudes. The "mixed" cases HiF$_{10.7}$-LoTEC-Sym/Asym primarily occur during nighttime, when the ionospheric E-layer vanishes and only the F-layer remains, and cluster at middle to high latitudes.

2.2 Datasets

We used data from the Meteorological Operational Satellite (MetOp-A) (e.g., Loiselet et al., 2000; Montenbruck et al., 2008; Von Engeln et al., 2009), which delivers data since the end of 2007. MetOp-A covers the period of our investigated solar cycle (2008 to 2015) with a reliable profile statistics number of about 700 profiles per day. As a complementary RO dataset we used data from the Gravity Recovery and Climate Experiment (GRACE) (e.g., Wickert et al., 2005; Beyerle et al., 2005), using the GRACE-A mission data in the same time range. For the processing we used the Wegener Center (WEGC) reference occultation processing system (rOPS) (Kirchengast et al., 2016, 2018; Schwarz et al., 2017, 2018; Innerkofler et al., 2020; Liu et al., 2020). MetOp-A and GRACE-A differ in their orbit altitudes, i.e., MetOp-A orbits at an altitude of about ∼820 km, while GRACE-A orbits at an altitude of about ∼470 km.

We applied the ionospheric kappa-correction to all RO profiles, to use them for assessment against the RO profiles with standard correction, and used the sampling approach to classify the data subsets. For the daily F$_{10.7}$ values we downloaded the data from Natural Resources Canada (`https://www.spaceweather.gc.ca/solarflux/sx-5-en.php`, last access: 28 October 2020). The vTEC maps were downloaded from the International Global Positioning System Service (IGS) center (`https://kb.igs.org/hc/en-us/articles/115003935351`, last access: 28 October 2020).

Using the F$_{10.7}$ and vTEC datasets (the latter including inbound and outbound vTEC's, as needed for), we sampled the RO profiles according into their respective category (i.e., low (Lo) or high (Hi) F$_{10.7}$ and vTEC values, and Sym/Asym f_{IA} values). We analyzed the RO datasets with typically inspecting the difference between the profiles with the higher order kappa-correction applied (labeled as RO$_\kappa$) against the profiles with just the first-order standard correction applied (labeled as RO).

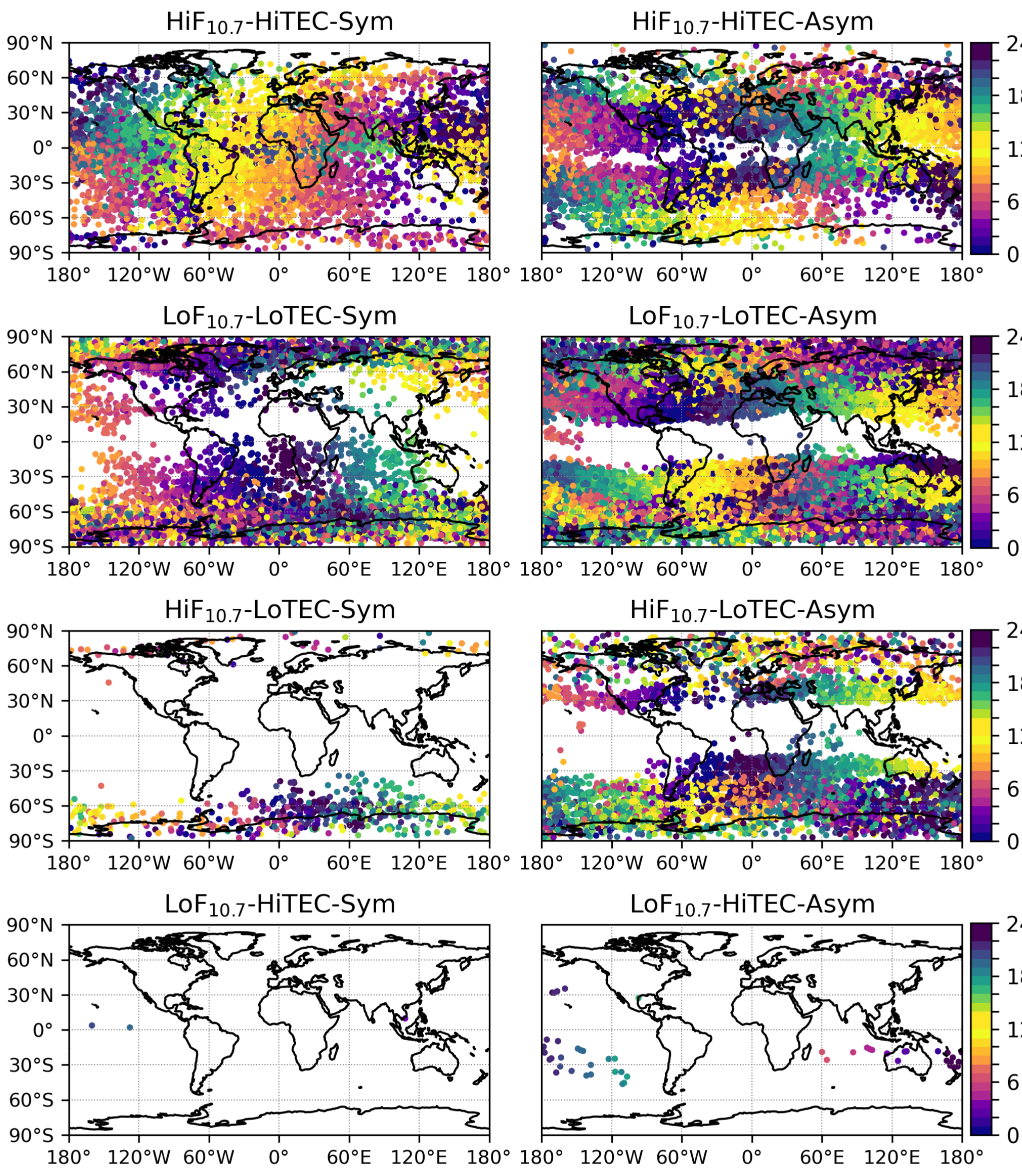

Figure 3. Geographic scatter plot map of the RO events of all 8 condition cases (see Table 2 for the case names and conditions), analyzed for the MetOp-A events from the years 2008 up to 2015. The RO events are marked as dots at their mean event location and the color indicates the local time at occurrence of the event (color bars on right-hand side).

For the intercomparison analysis with other quality datasets we used the European reanalyses ERA5 and ERA-Interim. In order to assess whether the kappa-correction improves the RO profiles, the comparison datasets need to show a very high quality at stratospheric altitudes. We consider the chosen reanalysis datasets to fulfill this requirement in a best possible manner though still marginally. However, based on initial previous validation studies by Liu et al. (2019), including SABER infrared limb sounder data, and by Danzer et al. (2020), including MIPAS middle-atmosphere infrared limb sounder data, we found these other observational satellite data are not sufficiently accurate.

Both the recent ERA5 reanalysis (Hersbach et al., 2018, 2020) and the predecessor reanalysis ERA-Interim (Dee et al., 2011) involve a four-dimensional variational data assimilation approach (4D-Var), based on the integrated forecasting system IFS of the European Centre for Medium-Range Weather Forecasts (ECMWF). ERA5 used an improved horizontal resolution of about 30 km and 137 vertical levels from the surface up to 0.01 hPa ($\sim$80 km), while ERA-Interim used a resolution of about 80 km and 60 vertical levels up to 0.1 hPa ($\sim$60 km). Both datasets fully cover the needed time period of 2008 to 2015.

Apart from the resolution and other model physics refinements, some differences in stratospheric temperatures from ERA5 compared to ERA-Interim are induced by advanced background covariance matrices, a changed bias adjustment for radiosonde data, and assimilation of COSMIC GNSS-RO bending angles from mid-2006 onwards (ERA-Interim from late-2009 onwards) (Hersbach et al., 2020). Overall slightly colder stratosphere temperatures are found in ERA5, which leads to ERA-Interim temperatures being in general globally about 1.5 K warmer than ERA5 near the stratopause (at 1 hPa level).

3 Results

3.1 Kappa-correction influence on atmospheric RO profiles

Here we present the overall kappa-correction performance results for the six characteristic condition cases. Figure 4 shows the magnitude of the correction term itself at bending angle profile level, while Figure 5 shows the impact at retrieved temperature level, based on the WEGC retrieval processing (subsection 2.2), illustrated for MetOp-A RO data ensembles.

The size of the kappa-correction term is clearly largest under high solar activity and high ionization (Hi$F_{10.7}$-HiTEC) under symmetric and asymmetric conditions (Fig. 4, left), with extreme deviations exceeding $-0.2\,\mu$rad under nearly symmetric conditions and even $-0.4\,\mu$rad under strongly asymmetric conditions. However, the mean value is found restricted to about -0.03 to $-0.05\,\mu$rad over the stratosphere and, interestingly, markedly smaller under asymmetric conditions. For low solar activity and ionization conditions, the mean correction is smaller than $-0.005\,\mu$rad. These mean results are in line with previous studies based on simulated data (Liu et al., 2015) and small observed data ensembles (Liu et al., 2020) and hence consolidate confidence in them, given the targeted large-size ensembles used here. The specific behavior revealed under different levels of ionization asymmetry, contrasting on an individual RO profile basis the kappa-correction term's mean-size behavior, is an interesting new finding that points to the need of future more detailed investigation under specific regional-scale conditions, as also recently suggested by Liu et al. (2020).

In retrieved stratospheric temperature profiles based on WEGC's rOPS refractivity and dry-air retrieval processing chain, these results lead to deviations against the use of standard correction of near -0.3 K for high ionization conditions in the upper stratosphere (40-45 km). In these cases, strong inbound/outbound asymmetry leads to outliers exceeding -2 K (-1 K under symmetry) (Figure 5). The correction-induced tem-

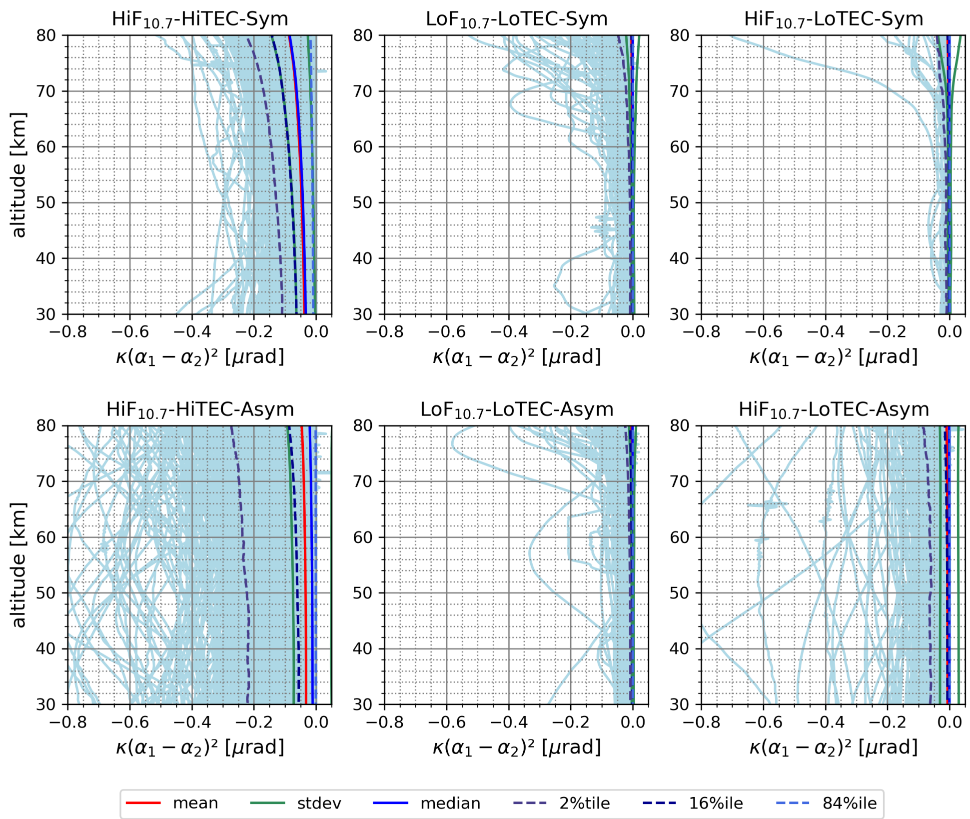

Figure 4. Size of the kappa-correction term in RO bending angle profiles (MetOp-A) over the upper stratosphere and mesosphere (30-80 km), comparing the six main characteristic condition cases of Table 2 (see panel titles for case identification; nearly-symmetric cases top, strongly-asymmetric cases bottom). For explanation of the six depicted statistics metrics, from mean to three selected percentile profiles, see the legend (bottom).

perature profile deviation increases with increasing altitude up to stratopause near heights (around 50 km), and decreases beyond into the mesosphere. This kind of propagating the deviation is an effect of dry-air retrieval processing (i.e., combined effect of hydrostatic integral and equation of state) as has been discussed by Schwarz et al. (2017) as part of introducing the rOPS uncertainty propagation from bending angle to dry-air temperature profiles. For the low solar activity and mixed case the impact of the error is rather small at both levels. In the case of $\mathrm{LoF}_{10.7}$-LoTEC-Asym, the mean temperature error in the upper stratosphere (40-45 km) is -0.0004 K, under symmetry the mean value lies by -0.0002 K. Illustrating again that symmetric conditions increase the mean value at bending angle and at temperature level.

Figure 6 illustrates the kappa-correction influence across the set of retrieved atmospheric profiles from bending angle to temperature, focusing on high solar and ionization conditions under near-symmetry where the mean deviations are strongest. Additionally we show both the mission ensembles from MetOp-A (upper part) and GRACE-A (lower part). This highlights how the kappa-correction-induced deviations propagate through the retrieval processing chain from bending angle (α) via refractivity (N) and pressure (p) to temperature (T). The GRACE-A ensemble exhibits a somewhat smaller

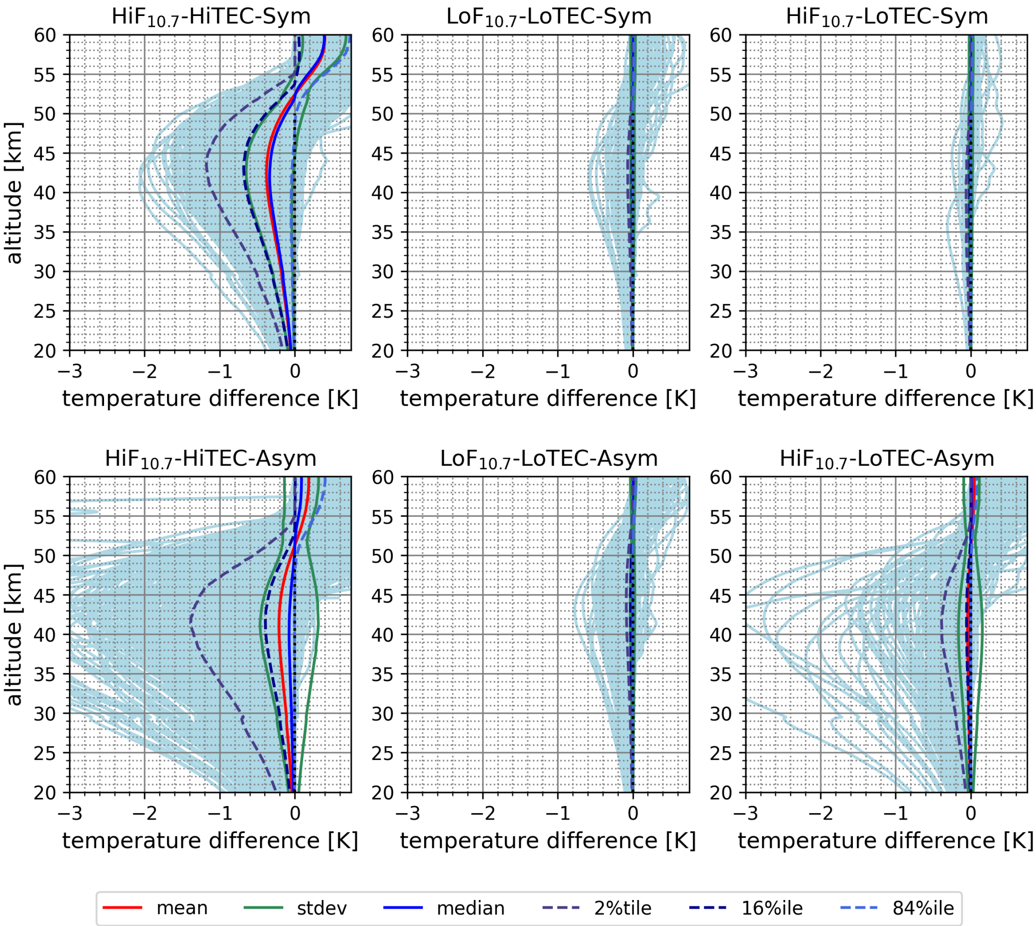

Figure 5. Kappa-correction-induced RO temperature profile deviations versus temperature profiles from standard bending angle correction (MetOp-A) from lower stratosphere to mesosphere (20-60 km), comparing the six main characteristic condition cases of Table 2 (see panel titles for case identification; nearly-symmetric cases top, strongly-asymmetric cases bottom). For explanation of the six depicted statistics metrics, from mean to three selected percentile profiles, see the legend (bottom).

diversity and spread of kappa-correction deviations than MetOp-A, which is likely related mostly to the overall smaller ensemble of profiles (cf. 2), capturing less extreme events.

The mean correction-term size at bending angle level is still very similar for both satellite missions (~ -0.03 to $-0.05\,\mu$rad). However, at temperature level we find that GRACE-A exhibits a smaller temperature deviation (for example, GRACE-A ~ -0.1 K), MetOp-A (~ -0.2 K, at around 35 km). Furthermore, the altitude level of the sign switch of the temperature deviation from negative to positive is about 5 km lower for GRACE-A (around 47 km, MetOp-A around 52 km). Both these effects of "damping down" the GRACE-A retrieved deviations compared to MetOp-A are presumably mainly induced by the different weighting of observation and background information in the bending angle statistical optimization step of the retrieval process before the Abelian transformation to refractivity, where MetOp-A receives highest weights of observed bending angles due to these data being assessed to have smallest observational errors (Schwarz et al., 2017; Angerer et al., 2017). This behavior is hence, as expected given that these different RO mission data properties apply in general, also found for the other characteristic cases including asymmetric conditions (not shown).

To visually summarize the influence of the kappa-correction term plus the subsequent retrieval process on RO temperature profiles, we show in Figure 7 a statistical results overview of all six characteristic condition cases for both MetOp-A and GRACE-A, in the form of box-and-whisker plots showing the median/quartiles/5-95percentile values for lower, middle, and upper stratosphere layers. In line with the discussion before we find that MetOp-A shows consistently higher deviations than GRACE-A, most visible in the upper stratosphere (40-45 km layer). For example, for MetOp-A and the high solar activity near-symmetry case, the temperature deviation increases from ~ -0.08 K to ~ -0.3 K, for the layers $20-25$ km to $40-45$ km, respectively. GRACE-A, on the other hand, stays below ~ -0.1 K. For the low-level condition cases (low solar activity and low ionization such as during night time and mostly at high latitudes), the temperature deviations stay generally smaller than ~ -0.02 K up to at least the 75^{th} percentile.

Overall this finding clearly signals the fact that the kappa-correction-induced temperature profile deviations in the stratosphere significantly depend on both the magnitude of the kappa-correction term itself as applied to the observed bending angle profile and on the observation-to-background weighting or other averaging/smoothing of bending angles, generally performed as a statistical initialization step (Li et al., 2015; Schwarz et al., 2017; Gleisner & Healy, 2013; Danzer et al., 2020) towards the subsequent refractivity and dry-air retrieval process.

Table 3 finally provides a summary of the deviation results found in this study for the kappa-correction-induced deviations at bending angle, refractivity, pressure, and temperature level across the stratosphere, focusing here on the high solar activity and ionization and near-symmetric case ($\text{HiF}_{10.7}$-HiTEC-Sym) as well as the high solar activity and low ionization strong-asymmetry case ($\text{HiF}_{10.7}$-LoTEC-Asym); the results for the other cases are found in Appendix A. We consider these beyond a concise numerical summary useful reference numbers also for further studies on the impact of RIEs and their correction in future, in particular when intercomparing different RIE correction methods and when studying more quantitatively the co-influence of the algorithmic choices in the subsequent retrieval process. An example of the relevance of this co-influence is evident from comparing the temperature-deviation results of this study to the predecessor study by Danzer et al. (2020), who used a so-called averaging-profile inversion (API) approach that retrieves climatological RO temperature profiles from averaged bending angle profiles: under high solar activity conditions with similar size of the kappa-correction term at bending angle level those mean stratospheric temperature deviations appear about twice as high compared to the mean deviations from this study.

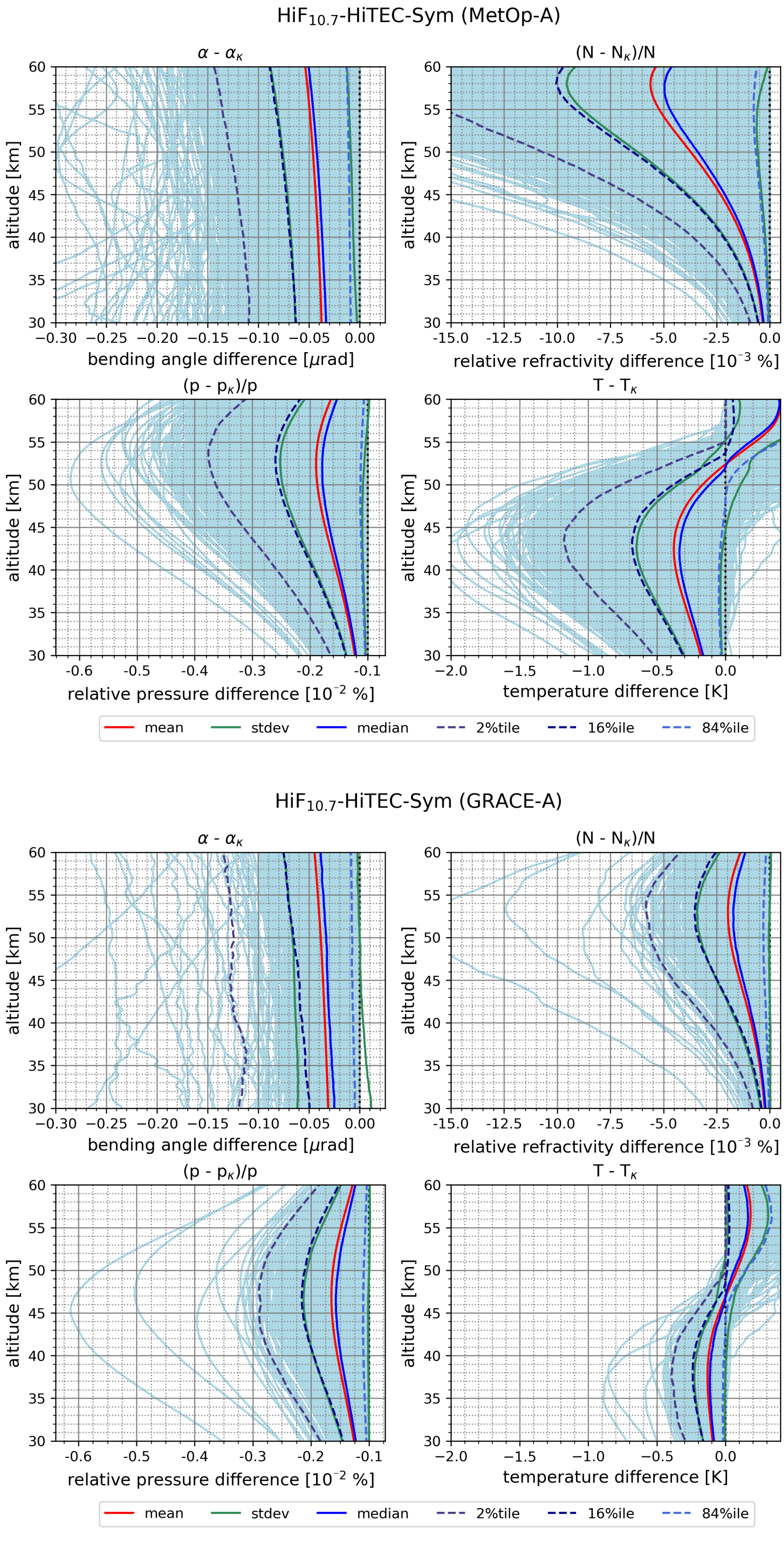

Figure 6. Kappa-correction-induced RO bending angle, refractivity, pressure, and temperature profile deviations versus standard-correction, showing the case for high solar and ionization conditions and near-symmetry (HiF$_{10.7}$-HiTEC-Sym) for MetOp-A (top part, upper four panels) and GRACE-A (bottom part, lower four panels), respectively. For explanation of the six depicted statistics metrics, from mean to three selected percentile profiles, see the legend (bottom).

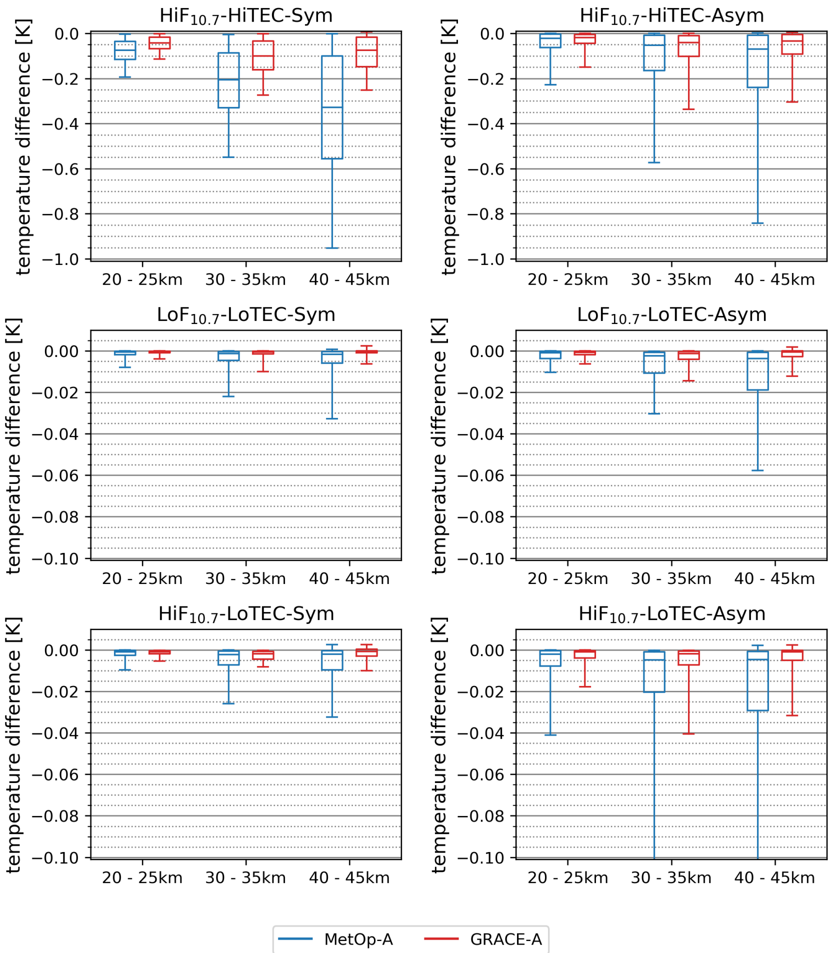

Figure 7. Statistics of the size of the kappa-correction-induced temperature deviations versus standard-correction, for all six characteristic condition cases, comparing the results for MetOp-A (blue) and GRACE-A (red) in representative lower (20-25 km), middle (30-35 km), and upper (40-45 km) stratosphere layers. The box-whisker bars show the median and the quartiles (box, median as horizontal line within) plus the 5^{th} and 95^{th} percentiles (whiskers). The y-axis range is zoomed into by a factor of 10 in the bottom two rows, to enable a legible illustration of the values for these low activity/ionization cases.

Table 3. Size of the kappa-correction term on bending angle (α profiles and of the kappa-correction-induced relative refractivity N, relative pressure p, and temperature T deviations (after WEGC's rOPS processing as used in this study), for lower, middle, and upper stratospheric layers and for both MetOp-A and GRACE-A (2008-2015 data). The characteristic condition cases of high solar activity/high ionization (mainly equatorial/daytime)/near-symmetry (HiF$_{10.7}$-HiTEC-Sym) and of high solar activity/low ionization (mainly non-equatorial/nighttime)/strong-asymmetry (HiF$_{10.7}$-LoTEC-Asym) are tabulated here (further cases in Appendix A).

HiF$_{10.7}$-HiTEC-Sym

	median				standard deviation			
MetOp-A	α [μrad]	N [10^{-3}%]	p [10^{-2}%]	T [K]	α [μrad]	N [10^{-3}%]	p [10^{-2}%]	T [K]
30-35 km	-0.034	-0.421	-0.131	-0.206	0.030	0.354	0.109	0.174
35-40 km	-0.036	-0.843	-0.205	-0.292	0.030	0.702	0.172	0.254
40-45 km	-0.038	-1.591	-0.292	-0.330	0.031	1.315	0.247	0.309
GRACE-A	α [μrad]	N [10^{-3}%]	p [10^{-2}%]	T [K]	α [μrad]	N [10^{-3}%]	p [10^{-2}%]	T [K]
30-35 km	-0.026	-0.295	-0.073	-0.101	0.035	0.325	0.072	0.094
35-40 km	-0.029	-0.569	-0.111	-0.113	0.034	0.603	0.103	0.111
40-45 km	-0.031	-0.993	-0.093	-0.077	0.033	1.007	0.129	0.093

HiF$_{10.7}$-LoTEC-Asym

	median				standard deviation			
MetOp-A	α [μrad]	N [10^{-3}%]	p [10^{-2}%]	T [K]	α [μrad]	N [10^{-3}%]	p [10^{-2}%]	T [K]
30-35 km	-0.001	-0.014	-0.004	-0.005	0.030	0.311	0.079	0.113
35-40 km	-0.001	-0.028	-0.006	-0.006	0.030	0.594	0.119	0.149
40-45 km	-0.001	-0.050	-0.008	-0.005	0.030	1.054	0.160	0.152
GRACE-A	α [μrad]	N [10^{-3}%]	p [10^{-2}%]	T [K]	α [μrad]	N [10^{-3}%]	p [10^{-2}%]	T [K]
30-35 km	-0.001	-0.008	-0.002	-0.002	0.014	0.115	0.023	0.026
35-40 km	-0.001	-0.013	-0.002	-0.002	0.012	0.205	0.031	0.028
40-45 km	-0.001	-0.023	-0.003	-0.001	0.011	0.328	0.037	0.020

3.2 Intercomparison of kappa-correction results with other datasets

Figure 8 analyzes RO temperature differences relative to comparison datasets from the European reanalyses ERA5 (top) and ERA-Interim (bottom), comparing RO-retrieved stratospheric temperature profile data statistics just with standard-correction (left) and with the kappa-correction applied (right), for the high solar activity and high ionization conditions with near-symmetry (Hi$F_{10.7}$-HiTEC-Sym). This intercomparison analysis indicates a decrease of the RIE by about $\sim$0.3 K due to applying the kappa-correction (very small and hence challenging to visually discern, though). This slight mean decrease appears against both the ERA5 and ERA-Interim datasets.

In general good agreement between the comparison datasets and RO temperature with both corrections is observed in the lower stratosphere. However, inspecting more closely, applying the kappa-correction increases the closeness of agreement by about $\sim$2 km in altitude, against the comparison datasets under this setup. An interesting trait of the temperature difference against ERA5 can be seen at $\sim$50 km. At this altitude the difference switches its sign and changes from positive to negative. This feature also occurs for the GRACE-A satellite data (not shown), but at a lower altitude of about 47 km. Another relevant feature of the temperature difference is its general increase with altitude, making it more difficult to attribute the reasons of deviations. In cases of low solar activity, the temperature difference between RO data and the comparison data are found somewhat smaller than in Figure 8 (not shown).

In order to visually summarize the intercomparison information, Figure 9 shows a box-and-whisker plot similar to Figure 7, here visualizing the differences of kappa-corrected (solid lines) and just standard-corrected (dashed lines) RO temperature data from MetOp-A (blue) and GRACE-A (red) across stratospheric layers against the ERA5 data; a twin figure comparing to ERA-Interim is found in Appendix A. The difference increases with altitude and the sign-change near the stratopause are well visible again. The box-whisker-plots reveal in addition that, in the lower and middle stratosphere, the median of the near-symmetry cases is slightly higher than the one of the asymmetry cases, whereas in the upper stratosphere it is the other way round. The comparison to ERA-Interim (Figure A1 in Appendix A) exhibits the same characteristics.

To sum up, the comparison against both reference datasets indicates a slight but discernible decrease of the temperature difference due to the application of the kappa-correction by about 0.2 K to 0.4 K, for cases with high solar activity and ionization. Even though the impact of the kappa-correction term differs in magnitude for both satellites and the temperature difference is in general smaller in GRACE-A data, it exhibits overall the same characteristics. Another difference between the satellite datasets is the altitude of the sign-change, which is higher for MetOp-A than for GRACE-A. The box-whisker plots showed in addition the influence symmetry/asymmetry conditions; in lower stratospheric layers symmetric conditions lead to a higher mean temperature difference than asymmetric conditions do. Overall we find, in line with the predecessor climatology-based study (Danzer et al., 2020) that the quality of reference datasets is still marginal for conclusive validation findings for such small effects like the kappa-correction influence of interest here.

We further inspected co-located profiles from the Michelson Interferometer for Passive Atmospheric Sounding (MIPAS) middle-atmosphere dataset, and also the Sounding of the Atmosphere using Broadband Emission Radiometry (SABER) with our RO datasets. However, these datasets were found not suitable for our analysis, as already was shown by Liu et al. (2020). MIPAS faces the practical problem of having no measurements in the most interesting time frame of high solar activity (data exist only to April 2012), while SABER has the feature of a cold bias of 3 K between 20 km to 35 km, and near $\pm$2 K between 35 km to 45 km altitude (see Innerkofler (2015)) which limits its utility as a reference dataset for the purpose of this study.

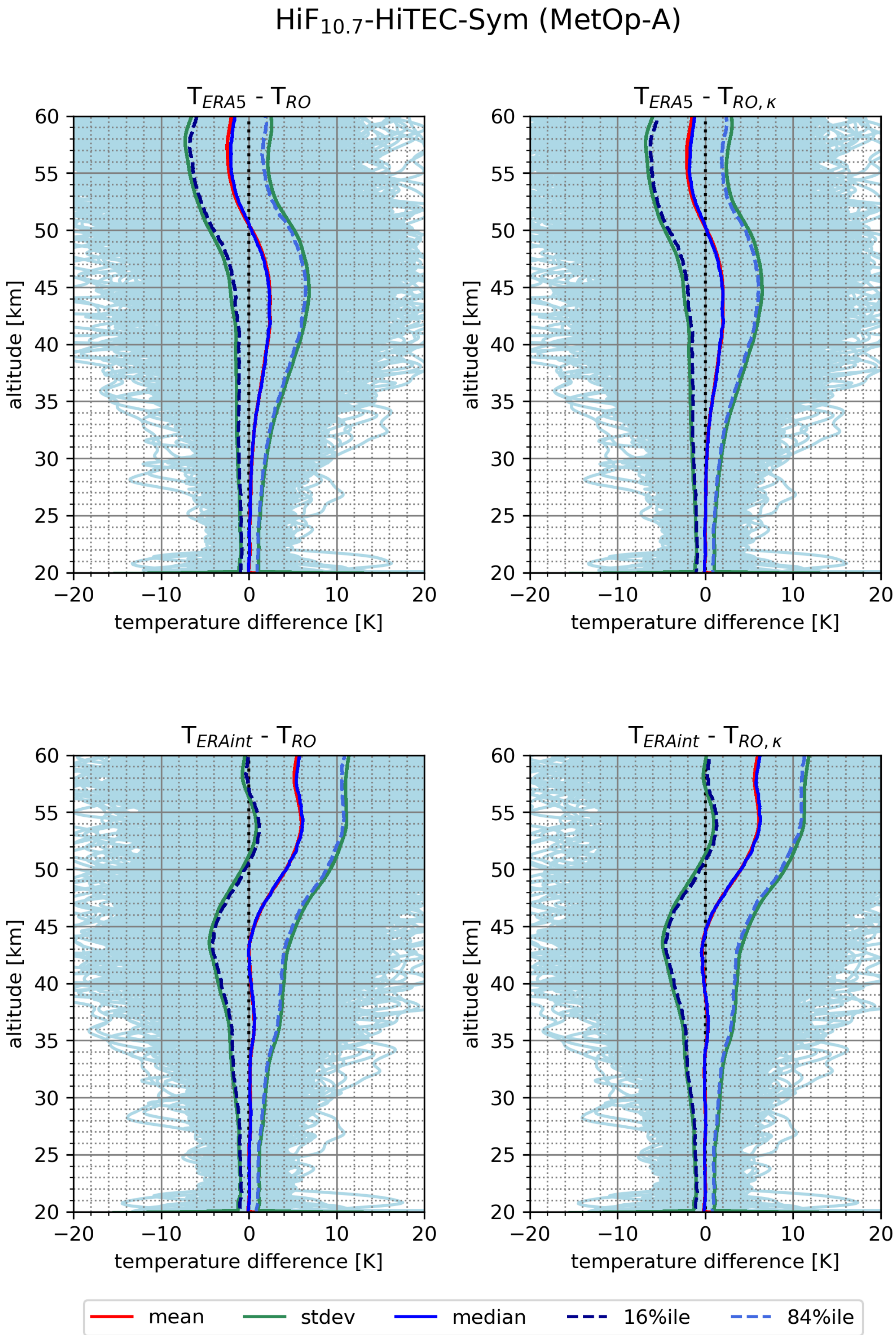

Figure 8. RO temperature profile statistics difference relative to ERA5 (top row) and ERA-Interim (bottom row) for the condition case HiF$_{10.7}$-HiTEC-Sym (MetOp-A). The difference statistics just with the standard correction (T_{RO}) (left column) and with the kappa-correction applied ($T_{RO,\kappa}$) (right column) are shown. The meaning of the depicted statistics, from mean to percentile profiles, can be found in the legend at bottom.

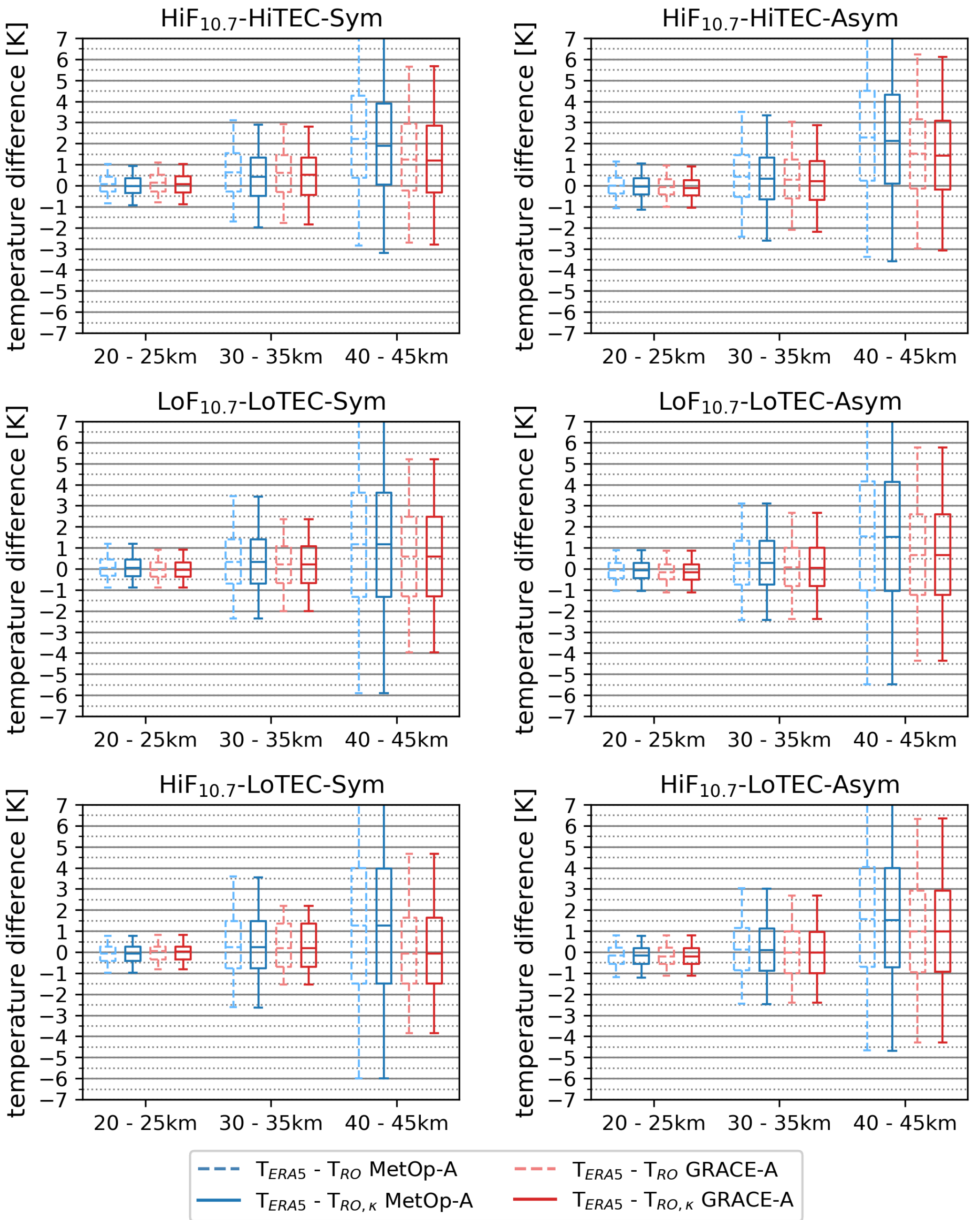

Figure 9. Temperature differences from intercomparison for all six sampling characteristic condition cases, comparing the results for MetOp-A (blue) and GRACE-A (red), just with the standard correction (dashed) and with the kappa-correction applied (solid), with ERA5 as comparison reference dataset. The box-whisker bars show the median and the quartiles (box, median as horizontal line within) plus the 5^{th} and 95^{th} percentiles (whiskers).

4 Conclusions

We analyzed the performance of the ionospheric kappa-correction of radio occultation profiles under diverse ionization and solar activity conditions. Overall, our results are consistent with the results from previous studies; the size of the kappa-correction strongly depends on the solar activity (e.g., Danzer et al., 2013; Liu et al., 2018). The kappa-correction term itself reached a mean value near 0.05 μrad under high conditions. Low solar activity and ionization conditions lead to a mean correction smaller than 0.005 μrad, which is in line with previous studies based on simulated data (Liu et al., 2015), and small observed data samples (Liu et al., 2020). For the kappa-correction induced RO temperature profile we observed an increase in the error at $\sim$45 km from low solar activity and low ionization to high solar activity and high ionization of around ~ -0.005 K to ~ -0.33 K for MetOp-A, while for GRACE-A the increase was from ~ -0.001 K to ~ -0.077 K, respectively, using the rOPS retrieval system.

We further observed a clear difference when investigating the impact of inbound/outbound ionospheric a-/symmetry. The impact of the kappa-correction for cases with low solar activity was larger for asymmetric inbound/outbound conditions. In the case of high solar activity, we found that symmetric inbound/outbound conditions lead to the strongest increase in the temperature error.

Our results indicate that the kappa-correction induced temperature profile deviations in the stratosphere strongly depend on two main factors. First, the magnitude of the kappa-correction term itself, as applied to the observed bending angle profile. Second, on the observation-to-background weighting or other averaging/smoothing of bending angles, which is in general performed prior to the refractivity and dry-air retrieval process.

We note that the differences that we observe in the perturbation of the RIE on temperature level for MetOp-A data, compared to the climatology study from Danzer et al. (2020), is about a factor of two. However, on bending angle level, the RIE is found to be the same. Hence, we conclude that the differences result from systematic differences in the processing and the retrieval system. Over the past years, there have been some ongoing changes in the rOPS system of the WEGC.

In the comparison of MetOp-A and GRACE-A satellite data, we observed on the one hand, different magnitudes for the kappa-correction, and on the other hand, a sign change from negative to positive, for both satellites. However, MetOp-A switched the sign at 52 km altitude, while GRACE-A already switched it 5 km below that. This change of the sign from negative to positive was also observed in the study by Vergados and Pagiatakis (2011), who used GPS RO events of CHAMP to show the impact of the second-order RIE on atmospheric parameters, however at altitudes between 25 km and 29 km. In that context we suggest to further investigate the impact of the orbit altitude of satellites on the residual ionospheric error. A multi-satellite analysis could give some additional insight on that specific feature.

The intercomparison analysis of the study showed the promising result that the application of the kappa-correction predominantly reduces the temperature error. As comparison datasets we used ERA5, and ERA-Interim. Under solar high conditions a decrease of the temperature error by a magnitude of $\sim$0.2 K to $\sim$0.4 K was found. In general the agreement between RO data and the comparison datasets are very good up to the middle stratosphere between about 30 km to 40 km, depending on the comparison dataset. In this setup, we found that the kappa-correction increased agreement on average by a height of $\sim$2 km, for both satellites (MetOp-A and GRACE-A), in the intercomparison analysis.

In general we note that the quality of reference datasets is still marginal for conclusive validation findings, which makes it difficult to validate possible improvements.

Especially since higher-order ionospheric corrections are quite small. Future investigations will have to include an analysis of the impact of Earth's geomagnetic field. As shown by Blagoveshchensky et al. (2018), sudden changes in the geomagnetic field can lead to a change in the TEC value of up to 67% of its quiet state. A possible way, to assess whether the kappa-correction accounts for such drastic changes in the geomagnetic field would be a comparison study to the bi-local correction approach, which includes the strength and the direction of the geomagnetic field (Liu et al., 2020).

The results of Blagoveshchensky et al. (2018) also show that the responses to sudden changes in the magnetic field are very different for different parts of the Earth. We therefore expect that differences average out globally in a climatological context. How changes in the magnetic field affect the quality of the kappa-correction on individual profiles, needs to be further investigated.

We arrive at the overall conclusion that the simple and fast correction of RO profiles on bending angle level via the ionospheric kappa-correction is a good alternative to more sophisticated approaches. Since additional background information always comes along with additional biases, the kappa-correction has the advantage of minimizing the number of such error sources. Despite its simplicity, the kappa-correction is an important method in operational applications and post-processing climatological analysis. With our findings we are encouraged to get one step closer to the extension of RO profiles to higher altitudes.

Appendix A Additional Table and Figure

Acknowledgments

We thank UCAR/CDAAC for providing MetOp-A and GRACE-A excess phase data, and the WEGC RO team for providing the OPSv5.6 retrieved profile data. The work was funded by the Austrian Science Fund (FWF) as part of a Hertha Firnberg-Project under grant T 757-N29 (NEWCLIM project) and supported also by the Austrian Research Promotion Agency projects ATROMSAF (ASAP-13 859771) and CLIMRECORD (ASAP-14 866020). The OPSv5.6 data are available at the website (`https://www.doi.org/10.25364/WEGC/OPS5.6:2020.1`, last access: 25 November 2020). The ERA5 and ERA-Interim reference data can be downloaded at (`https://cds.climate.copernicus.eu/#!/search?text=ERA5&type=dataset`) and (`https://apps.ecmwf.int/datasets/`). The $F_{10.7}$ solar flux values were downloaded from Natural Resources Canada (`https://www.spaceweather.gc.ca/solarflux/sx-5-en.php`, last access: 13 May 2020), the TEC values were extracted from the International Global Positioning System Service (IGS) center (`https://kb.igs.org/hc/en-us/articles/115003935351`, last access: 23 September 2020).

References

Angerer, B., Ladstädter, F., Scherllin-Pirscher, B., Schwärz, M., Steiner, A. K., Foelsche, U., & Kirchengast, G. (2017). Quality aspects of the wegener center multi-satellite gps radio occultation record opsv5. 6. *Atmospheric Measurement Techniques*, *10*(12), 4845–4863. doi: 10.5194/amt-2017-225

Angling, M. J., Elvidge, S., & Healy, S. B. (2018). Improved model for correcting the ionospheric impact on bending angle in radio occultation measurements. *Atmospheric Measurement Techniques*, *11*, 2213-2224. doi: 10.5194/amt-11-2213-2018

Anthes, R. (2011). Exploring earth's atmosphere with radio occultation: contributions to weather, climate and space weather. *Atmospheric Measurement Techniques*, *4*(6), 1077.

Table A1. Size of the kappa-correction term on bending angle (α profiles and of the kappa-correction-induced relative refractivity N, relative pressure p, and temperature T deviations (after WEGC's rOPS processing as used in this study), for lower, middle, and upper stratospheric layers and for both MetOp-A and GRACE-A (2008-2015 data). The characteristic condition cases HiF$_{10.7}$-HiTEC-Asym, HiF$_{10.7}$-LoTEC-Sym, LoF$_{10.7}$-LoTEC-Asym, and LoF$_{10.7}$-LoTEC-Sym are tabulated here..

HiF$_{10.7}$-HiTEC-Asym								
	median				standard deviation			
MetOp-A	α [μrad]	N [10^{-3}%]	p [10^{-2}%]	T [K]	α [μrad]	N [10^{-3}%]	p [10^{-2}%]	T [K]
30-35 km	-0.011	-0.131	-0.037	-0.053	0.061	0.636	0.171	0.249
35-40 km	-0.011	-0.255	-0.056	-0.071	0.060	1.234	0.262	0.343
40-45 km	-0.012	-0.464	-0.078	-0.071	0.061	2.241	0.364	0.375
GRACE-A	α [μrad]	N [10^{-3}%]	p [10^{-2}%]	T [K]	α [μrad]	N [10^{-3}%]	p [10^{-2}%]	T [K]
30-35 km	-0.012	-0.127	-0.032	-0.042	0.049	0.484	0.115	0.156
35-40 km	-0.012	-0.254	-0.046	-0.048	0.049	0.921	0.168	0.191
40-45 km	-0.013	-0.443	-0.058	-0.035	0.049	1.605	0.216	0.164

HiF$_{10.7}$-LoTEC-Sym								
	median				standard deviation			
MetOp-A	α [μrad]	N [10^{-3}%]	p [10^{-2}%]	T [K]	α [μrad]	N [10^{-3}%]	p [10^{-2}%]	T [K]
30-35 km	-0.0003	-0.007	-0.002	-0.002	0.003	0.047	0.012	0.017
35-40 km	-0.0003	-0.013	-0.003	-0.003	0.004	0.115	0.012	0.020
40-45 km	-0.0003	-0.022	-0.004	-0.002	0.005	0.206	0.021	0.024
GRACE-A α [μrad]	N [10^{-3}%]	p [10^{-2}%]	T [K]	α [μrad]	N [10^{-3}%]	p [10^{-2}%]	T [K]	
30-35 km	-0.0005	-0.008	-0.002	-0.002	0.004	0.040	0.005	0.004
35-40 km	-0.0005	-0.017	-0.003	-0.001	0.004	0.061	0.005	0.007
40-45 km	-0.0005	-0.024	-0.003	-0.001	0.002	0.057	0.006	0.007

LoF$_{10.7}$-LoTEC-Asym								
	median				standard deviation			
MetOp-A	α [μrad]	N [10^{-3}%]	p [10^{-2}%]	T [K]	α [μrad]	N [10^{-3}%]	p [10^{-2}%]	T [K]
30-35 km	-0.0003	-0.006	-0.002	-0.002	0.003	0.033	0.010	0.016
35-40 km	-0.0003	-0.011	-0.003	-0.003	0.003	0.066	0.016	0.023
40-45 km	-0.0004	-0.021	-0.004	-0.004	0.003	0.125	0.023	0.029
GRACE-A	α [μrad]	N [10^{-3}%]	p [10^{-2}%]	T [K]	α [μrad]	N [10^{-3}%]	p [10^{-2}%]	T [K]
30-35 km	-0.0004	-0.005	-0.001	-0.001	0.003	0.025	0.006	0.008
35-40 km	-0.0004	-0.009	-0.002	-0.001	0.003	0.051	0.009	0.010
40-45 km	-0.0004	-0.016	-0.002	-0.001	0.003	0.089	0.011	0.009

LoF$_{10.7}$-LoTEC-Sym								
	median				standard deviation			
MetOp-A	α [μrad]	N [10^{-3}%]	p [10^{-2}%]	T [K]	α [μrad]	N [10^{-3}%]	p [10^{-2}%]	T [K]
30-35 km	-0.0002	-0.004	-0.001	-0.001	0.004	0.037	0.009	0.014
35-40 km	-0.0002	-0.007	-0.002	-0.002	0.004	0.071	0.015	0.021
40-45 km	-0.0002	-0.013	-0.002	-0.002	0.003	0.133	0.021	0.024
GRACE-A	α [μrad]	N [10^{-3}%]	p [10^{-2}%]	T [K]	α [μrad]	N [10^{-3}%]	p [10^{-2}%]	T [K]
30-35 km	-0.0002	-0.003	-0.001	-0.001	0.002	0.016	0.003	0.004
35-40 km	-0.0002	-0.005	-0.001	-0.001	0.002	0.028	0.005	0.006
40-45 km	-0.0002	-0.008	-0.001	-0.000	0.002	0.047	0.006	0.006

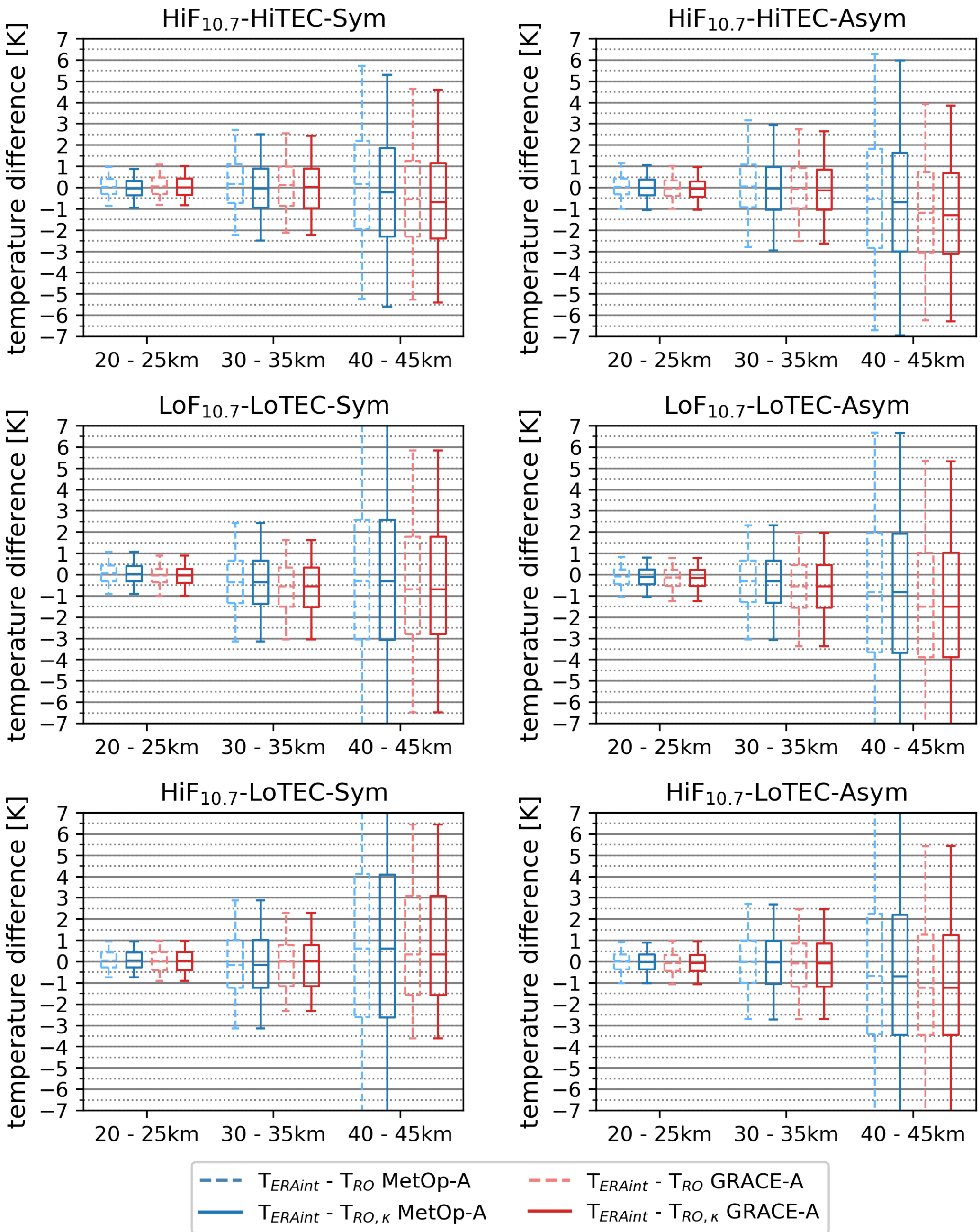

Figure A1. Temperature differences from intercomparison for all six sampling characteristic condition cases, comparing the results for MetOp-A (blue) and GRACE-A (red), just with the standard correction (dashed) and with the kappa-correction applied (solid), with ERA-Interim as comparison reference dataset. The box-whisker bars show the median and the quartiles (box, median as horizontal line within) plus the 5^{th} and 95^{th} percentiles (whiskers).

Ao, C. O., Schreiner, W. B., & Wickert, J. (2003). *First report on the CHAMP radio occultation intercomparison study* (Tech. Rep.). JPL.

Beyerle, G., Schmidt, T., G., G. M., Heise, S., Wickert, J., & Reigber, C. (2005). GPS radio occultation with GRACE: Atmospheric profil-ing utilizing the zero difference technique. *Geophysical Research Letters*, *32*(L13806). doi: 10.1029/2005GL023109

Blagoveshchensky, D., Maltseva, O., & Sergeeva, M. (2018, 08). Impact of magnetic storms on the global tec distribution. *Annales Geophysicae*, *36*, 1057-1071. doi: 10.5194/angeo-36-1057-2018

Cardinali, C. (2009). Monitoring the observation impact on the short-range forecast. *Quarterly Journal of the Royal Meteorological Society*, *135*(638), 239–250. doi: 10.1002/qj.366

Cucurull, L. (2010). Improvement in the use of an operational constellation of gps radio occultation receivers in weather forecasting. *Weather and Forecasting*, *25*(2), 749–767. doi: 10.1175/2009WAF2222302.1

Danzer, J., Healy, S., & Culverwell, I. (2015). A simulation study with a new residual ionospheric error model for GPS radio occultation climatologies. *Atmospheric Measurement Techniques*, *8*(8), 3395–3404. doi: 10.5194/amt-8-3395-2015

Danzer, J., Scherllin-Pirscher, B., & Foelsche, U. (2013). Systematic residual ionospheric errors in radio occultation data and a potential way to minimize them. *Atmospheric Measurement Techniques*, *6*(8), 2169–2179. doi: 10.5194/amt-6-2169-2013

Danzer, J., Schwaerz, M., Kirchengast, G., & Healy, S. (2020). Sensitivity analysis and impact of the kappa-correction of residual ionospheric biases on radio occultation climatologies. *Earth and Space Science*, *7*(7), e2019EA000942. doi: 10.1029/2019EA000942

Dee, D. P., Uppala, S., Simmons, A., Berrisford, P., Poli, P., Kobayashi, S., . . . others (2011). The ERA-Interim reanalysis: Configuration and performance of the data assimilation system. *Quarterly Journal of the royal meteorological society*, *137*(656), 553–597. doi: 10.1002/qj.828

Foelsche, U., Kirchengast, G., & Steiner, A. K. (2003). Global climate monitoring based on CHAMP/GPS radio occultation data. In C. Reigber, H. Lhr, & P. Schwintzer (Eds.), *First CHAMP mission results for gravity, magnetic and atmospheric studies* (p. 397-407). Springer. doi: 10.1007/978-3-540-38366-6_55

Foelsche, U., Scherllin-Pirscher, B., Ladstädter, F., Steiner, A. K., & Kirchengast, G. (2011). Refractivity and temperature climate records from multiple radio occultation satellites consistent within 0.05 %. *Atmospheric Measurement Techniques*, *4*, 2007-2018. doi: 10.5194/amt-4-2007-2011

Gleisner, H., & Healy, S. B. (2013). A simplified approach for generating GNSS radio occultation refractivity climatologies. *Atmospheric Measurement Techniques*, *6*(1), 121–129. doi: 10.5194/amt-6-121-2013

Gobiet, A., Kirchengast, G., Manney, G. L., Borsche, M., Retscher, C., & Stiller, G. (2007). Retrieval of temperature profiles from CHAMP for climate monitoring: Intercomparison with Envisat MIPAS and GOMOS and different atmospheric analyses. *Atmospheric Chemistry and Physics*, *7*, 3519-3536.

Hajj, G. A., Kursinski, E. R., Romans, L. J., Bertiger, W. I., & Leroy, S. S. (2002). A technical description of atmospheric sounding by GPS occultation. *Journal of Atmospheric and Solar-Terrestrial Physics*, *64*(4), 451-469. doi: 10.1016/S1364-6826(01)00114-6

Healy, S., & Culverwell, I. (2015). A modification to the standard ionospheric correction method used in GPS radio occultation. *Atmospheric Measurement Techniques*, *8*(8), 3385–3393. doi: 10.5194/amt-8-3385-2015

Healy, S., & Thépaut, J. N. (2006). Assimilation experiments with CHAMP GPS radio occultation measurements. *Quarterly Journal of the Royal Meteorological Society*, *132*(615), 605-623. doi: 10.1256/qj.04.182

Hersbach, H., Bell, B., Berrisford, P., Hirahara, S., Horányi, A., Muñoz-Sabater, J., … others (2020). The era5 global reanalysis. *Quarterly Journal of the Royal Meteorological Society*, *146*(730), 1999–2049.

Hersbach, H., de Rosnay, P., Bell, B., Schepers, D., Simmons, A., Soci, C., … Zuo, H. (2018). *Operational global reanalysis: progress, future directions and synergies with NWP* (ERA Report Series No. 27). Reading, UK. doi: 10.21957/tkic6g3wm

Ho, S.-P., Hunt, D., Steiner, A. K., Mannucci, A. J., Kirchengast, G., Gleisner, H., … Gorbunov, M. (2012). Reproducibility of GPS radio occultation data for climate monitoring: Profile-to-profile inter-comparison of CHAMP climate records 2002 to 2008 from six data centers. *Journal of Geophysical Research*, *117*, D18111. doi: 10.1029/2012JD017665

Hoque, M. M., & Jakowski, N. (2008). Mitigation of higher order ionospheric effects on GNSS users in europe. *GPS solutions*, *12*(2), 87–97.

Innerkofler, J. (2015). *Evaluation of the climate utility of radio occultation data in the upper stratosphere and mesosphere (msc thesis).* Sci. Rep. 65-2015, 154 pp., Wegener Center Verlag, Graz, Austria.

Innerkofler, J., Kirchengast, G., Schwärz, M., Pock, C., Jäggi, A., Andres, Y., & Marquardt, C. (2020). Precise orbit determination for climate applications of gnss radio occultation including uncertainty estimation. *Remote Sensing*, *12*(7), 1180. doi: 10.3390/rs12071180

Kedar, S., Hajj, G. A., Wilson, B. D., & Heflin, M. B. (2003). The effect of the second order gps ionospheric correction on receiver positions. *Geophysical Research Letters*, *30*(16). doi: 10.1029/2003GL017639

Kirchengast, G., Schwärz, M., Angerer, B., Schwarz, J., Innerkofler, J., Proschek, V., … Rieckh, T. (2018). *Reference OPS DAD—Reference Occultation Processing System (rOPS) Detailed Algorithm Description* (Tech. Rep. for ESA and FFG No. 1/2018, Doc-Id: WEGC–rOPS–2018–TR01, Issue 2.0). Wegener Center, University of Graz.

Kirchengast, G., Schwärz, M., Schwarz, J., Scherllin-Pirscher, B., Pock, C., Innerkofler, J., … Ladstädter, F. (2016). *The Reference Occultation Processing System approach to interpret GNSS radio occultation as SI-traceable planetary system refractometer.* presented at OPAC-IROWG International Workshop, 8-14 September 2016. Retrieved from `http://wegcwww.unigraz.at/opacirowg2016/data/public/files/opacirowg206_Gottfried_Kirchengast_presentation_261.pdf`

Kursinski, E. R., Hajj, G. A., Schofield, J. T., Linfield, R. P., & Hardy, K. R. (1997). Observing Earth's atmosphere with radio occultation measurements using the Global Positioning System. *Journal of Geophysical Research*, *102*, 23429-23465. doi: 10.1029/97JD01569

Ladreiter, H. P., & Kirchengast, G. (1996). GPS/GLONASS sensing of the neutral atmosphere: Model-independent correction of ionospheric influences. *Radio Sci.*, *31*, 877-891. doi: 10.1029/96RS01094

Li, Y., Kirchengast, G., Scherllin-Pirscher, B., Norman, R., Y. B. Yuan, J. F., Schwaerz, M., & Zhang, K. (2015). Dynamic statistical optimization of GNSS radio occultation bending angles: advanced algorithm and performance analysis. *Atmospheric Measurement Techniques*, *8*, 3447–3465. doi: 10.5194/amt-8-3447-2015

Liu, C., Kirchengast, G., Sun, Y., Zhang, K., Norman, R., Schwaerz, M., … Li, Y. (2018). Analysis of ionospheric structure influences on residual ionospheric errors in gnss radio occultation bending angles based on ray tracing simulations. *Atmospheric Measurement Techniques*, *11*(4), 2427–2440. doi: 10.5194/amt-11-2427-2018

Liu, C., Kirchengast, G., Syndergaard, S., Schwaerz, M., & Danzer, J. (2019). *Higher-order ionospheric correction of bending angles accounting for ionospheric asymmetry and evaluation of correction methods* (Tech. Rep.). ROM-SAF. Retrieved from `romsaf.org/visiting_scientist.php` (CDOP-3 Visiting Scientist Report 34. Ref: SAF/ROM/DMI/REP/VS/34, 56 pp.)

Liu, C., Kirchengast, G., Syndergaard, S., Schwaerz, M., & Danzer, J. (2020). New higher-order correction of GNSS RO bending angles accounting for ionospheric asymmetry: evaluation of performance and added value. *Remote Sensing*, *12*, 3637–3660. doi: 10.3390/rs12213637

Liu, C., Kirchengast, G., Zhang, K., Norman, R., Li, Y., Zhang, S., ... others (2013). Characterisation of residual ionospheric errors in bending angles using GNSS RO end-to-end simulations. *Advances in Space Research*, *52*(5), 821–836. doi: 10.1016/j.asr.2013.05.021

Liu, C., Kirchengast, G., Zhang, K., Norman, R., Li, Y., Zhang, S., ... Tan, Z. (2015). Quantifying residual ionospheric errors in GNSS radio occultation bending angles based on ensembles of profiles from end-to-end simulations. *Atmospheric Measurement Techniques*, *8*(7), 2999–3019. doi: 10.5194/amt-8-2999-2015

Loiselet, M., Stricker, N., Menard, Y., & Luntama, J.-P. (2000). GRAS—MetOp's GPS-based atmospheric sounder. *ESA Bulletin*, *102*, 38-44.

Mannucci, A., Ao, C., Pi, X., & Iijima, B. (2011). The impact of large scale ionospheric structure on radio occultation retrievals. *Atmospheric Measurement Techniques*, *4*(12), 2837–2850. doi: 10.5194/amt-4-2837-2011

Montenbruck, O., Andres, Y., Bock, H., van Helleputte, T., van den Ijssel, J., Loiselet, M., ... Yoon, Y. (2008). Tracking and orbit determination performance of the GRAS instrument on metop-A. *GPS solutions*, *12*(4), 289–299. doi: 10.1007/s10291-008-0091-2

Rieder, M. J., & Kirchengast, G. (2001). Error analysis and characterization of atmospheric profiles retrieved from GNSS occultation data. *Journal of Geophysical Research*, *106*, 31755-31770.

Schwarz, J., Kirchengast, G., & Schwaerz, M. (2017, 05). Integrating uncertainty propagation in gnss radio occultation retrieval: from bending angle to dry-air atmospheric profiles. *Earth Space Sci.*, *4*(4), 200–228. doi: 10.1002/2016EA000234

Schwarz, J., Kirchengast, G., & Schwaerz, M. (2018). Integrating uncertainty propagation in gnss radio occultation retrieval: from excess phase to atmospheric bending angle profiles. *Atmospheric Measurement Techniques*, *11*(5), 2601–2631. doi: 10.5194/amt-11-2601-2018

Steiner, A., Hunt, D., Ho, S.-P., Kirchengast, G., Mannucci, A. J., Scherllin-Pirscher, B., ... Wickert, J. (2013). Quantification of structural uncertainty in climate data records from gps radio occultation. *Atmospheric Chemistry and Physics*, *13*(3), 1469–1484. doi: 10.5194/acp-13-1469-2013

Steiner, A., Kirchengast, G., Foelsche, U., Kornblueh, L., Manzini, E., & Bengtsson, L. (2001). GNSS occultation sounding for climate monitoring. *Physics and Chemistry of the Earth, Part A: Solid Earth and Geodesy*, *26*(3), 113-124. doi: 10.1016/S1464-1895(01)00034-5

Steiner, A., Lackner, B., Ladstädter, F., Scherllin-Pirscher, B., Foelsche, U., & Kirchengast, G. (2011). Gps radio occultation for climate monitoring and change detection. *Radio Science*, *46*(06), 1–17. doi: 10.1029/2010RS004614

Steiner, A. K., & Kirchengast, G. (2005). Error analysis of GNSS radio occultation data based on ensembles of profiles from end-to-end simulations. *Journal of Geophysical Research*, *110*. doi: 10.1029/2004JD005251

Syndergaard, S. (2000). On the ionosphere calibration in GPS radio occultation measurements. *Radio Science*, *35*(3), 865-883. doi: 10.1029/1999RS002199

Syndergaard, S. (2002). A new algorithm for retrieving GPS radio occultation total electron content. *Geophysical research letters*, *29*(16), 55–1.

Syndergarrd, S., & Kirchengast, G. (2019). *A bi-local estimation approach for residual ionospheric correction of radio occultation bending angles.* poster presented at EUMETSAT ROM SAF-IROWG International Workshop, 19-25 September 2019, Fri, 20 Sept., Poster P23. Retrieved from `https://www.romsaf.org/romsaf-irowg-2019/en/content/21/program-agenda-by-day`

Vergados, P., & Pagiatakis, S. D. (2010). First estimates of the second-order ionospheric effect on radio occultation observations. *Journal of Geophysical Research: Space Physics*, *115*(A7). doi: 10.1029/2009JA015161

Vergados, P., & Pagiatakis, S. D. (2011). Latitudinal, solar, and vertical variability of higher-order ionospheric effects on atmospheric parameter retrievals from radio occultation measurements. *Journal of Geophysical Research: Space Physics*, *116*(A9). doi: 10.1029/2011JA016573

Von Engeln, A., Healy, S., Marquardt, C., Andres, Y., & Sancho, F. (2009). Validation of operational GRAS radio occultation data. *Geophysical Research Letters*, *36*(17). doi: 10.1029/2009GL039968

Vorob'ev, V. V., & Krasil'nikova, T. G. (1994). Estimation of the accuracy of the atmospheric refractive index recovery from Doppler shift measurements at frequencies used in the NAVSTAR system. *Izvestiya, Atmospheric and Oceanic Physics*, *29*, 602-609.

Wickert, J., Beyerle, G., König, R., Heise, S., Grunwaldt, L., Michalak, G., . . . Schmidt, T. (2005). GPS radio occultation with CHAMP and GRACE: A first look at a new and promising satellite configuration for global atmospheric sounding. *Annales Geophysicae*, *23*, 653-658. doi: https://doi.org/10.5194/angeo-23-653-2005

Wickert, J., Reigber, C., Beyerle, G., König, R., Marquardt, C., Schmidt, T., . . . Hocke, K. (2001). Atmosphere sounding by GPS radio occultation: First results from CHAMP. *Geophysical Research Letters*, *28*(17), 3263-3266. doi: 10.1029/2001GL013117

Zeng, Z., Sokolovskiy, S., Schreiner, W. S., & Hunt, D. (2019). Representation of vertical atmospheric structures by radio occultation observations in the upper troposphere and lower stratosphere: Comparison to high-resolution radiosonde profiles. *Journal of Atmospheric and Oceanic Technology*, *36*(4), 655–670. doi: 10.1175/JTECH-D-18-0105.1